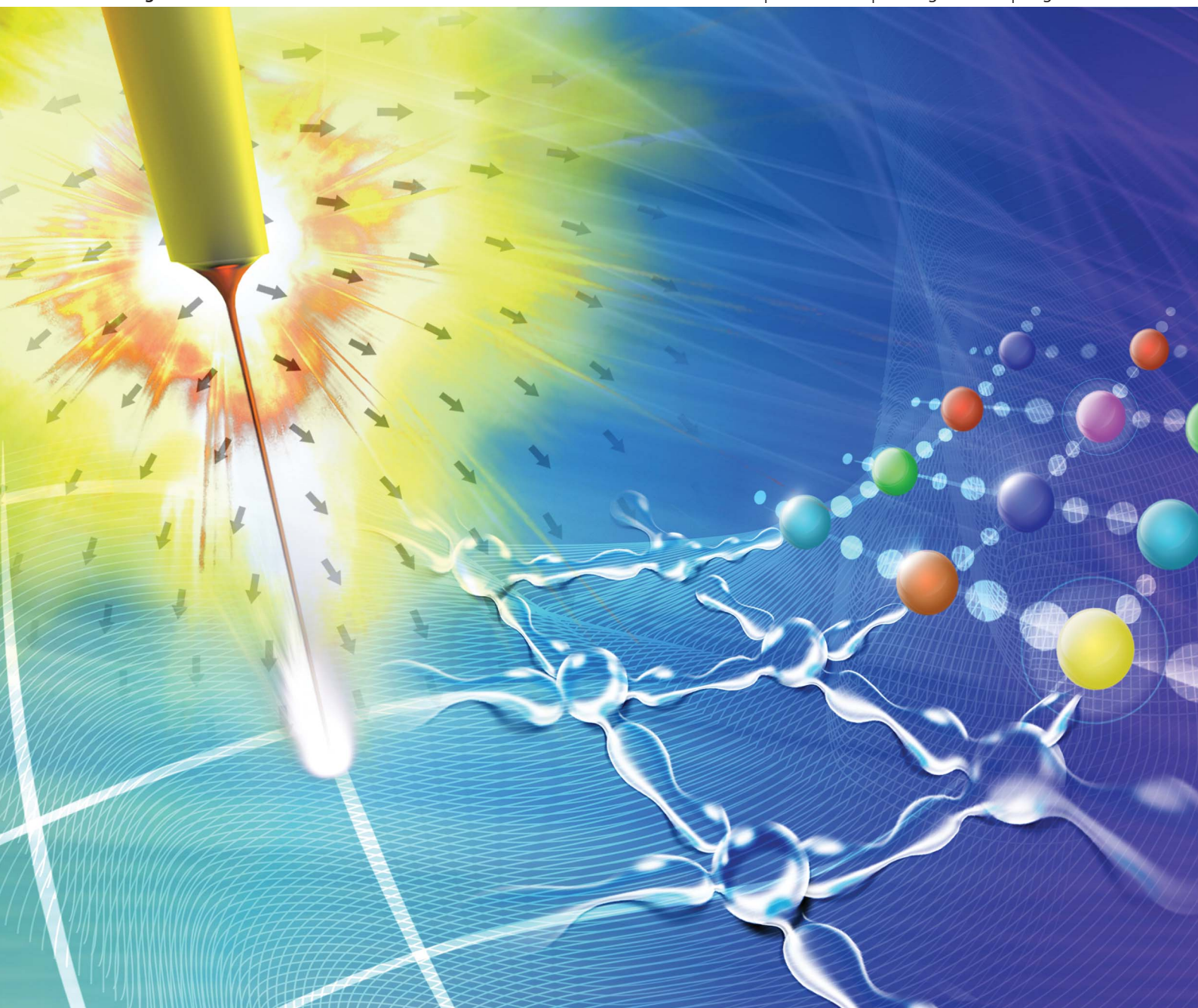


Soft Matter

www.rsc.org/softmatter

Volume 8 | Number 32 | 28 August 2012 | Pages 8243–8524



ISSN 1744-683X

RSC Publishing

PAPER

YongAn Huang, Zhouping Yin *et al.*
Controllable self-organization of colloid microarrays based on finite length effects of electrospun ribbons

Cite this: *Soft Matter*, 2012, **8**, 8302

www.rsc.org/softmatter

PAPER

Controllable self-organization of colloid microarrays based on finite length effects of electrospun ribbons

YongAn Huang,* Xiaomei Wang, Yongqing Duan, Ningbin Bu and Zhouping Yin*

Received 7th March 2012, Accepted 11th June 2012

DOI: 10.1039/c2sm25535a

This paper presents a mechano-electrospinning (MES)-assisted surface-tension driven self-organization to provide a possible route towards inexpensive generation of large-scale ordered microarrays in a controllable manner. To control the self-organization driven by surface tension and Plateau–Rayleigh instability, finite length effects are utilized to manipulate the self-organizing processes and adjust the competition between nucleation and free surface instability. We introduce fine ribbon-lattices to determine the boundary conditions of ribbons to make use of the finite length effects. The ribbon-lattices are electrodeposited precisely by MES, borrowing ideas from the “Chinese kite”, by involving the mechanical drawing force and the electric field force. Then the samples are transferred to a moisture-rich environment in which the ribbons absorb water vapour and become liquid lines. Surface instability emerges and leads the liquid lines to controllable self-organization. We uncover the controllable area to manipulate the self-organization behavior. A uniform or hierarchical microarray with a specific position, gap and droplet-size can be generated in a continuously tunable manner. This bottom-up method provides a digital approach for the fabrication of large-scale ordered microarrays and micropatterns.

1. Introduction

The controllable fabrication of functional microarrays is important in applications, including organic semiconductors and flexible electronics,^{1–3} bio-related and medicinal research ranging from biomolecule sensing and stimulation^{4,5} to cell and tissue engineering,^{6,7} the generation of masks and templates⁸ and the production of optical components such as microlens arrays,⁹ where a hierarchical microarray of colloid/polymeric material needs to be deposited on a rigid/flexible substrate and allowed to solidify by thermal, chemical, or photochemical means. A simple and inexpensive method is presented, employing passive mechanisms to generate a large-area ordered and hierarchical microarray with only additive solution-based processes. Contact approaches, such as dip-pen lithography¹⁰ and soft lithography,¹¹ have been commonly employed for processing suspensions on the nanoscale, but require strictly controlled atmospheres and are relatively costly. Non-contact techniques based on ink-jet printing have increasingly attracted attention from research and industrial communities due to their low-cost, high-efficiency, and environmentally friendly features.^{12–14} Traditional ink-jet printing is impractical for reaching a resolution smaller than 20 μm . The e-jet can be used to generate several micrometer or

submicrometer droplets in a drop-on-demand style, but by use of a high-resolution print-head with an inner diameter of a few micrometers.¹⁵ Notably, neither ink-jet nor e-jet has the flexibility to generate various droplets in a continuously tunable manner. Their adoption is dominated by the following challenges: (1) avoiding or eliminating jamming problems resulting from the high concentration solution in high-resolution printing; (2) improving the controllability of droplet-size and position in a parallel and highly-efficient manner; (3) fabricating hierarchical or different resolution microarrays or micropatterns in a continuously tunable manner.

The solution-based self-organization processes presented in many different inorganic, organic, and biological systems at various length scales give rise to specific intrinsic physical properties and offer lower production costs, reduced energy consumption, and a smaller environmental burden.^{3,16} One challenge in self-organization/self-assembly is that it is difficult to determine the behavior by changing many of the parameters.¹⁷ It was shown that droplets can be forced into certain desired microstructures or micropatterns by means of a pre-designed system, such as custom topographic and wettability patterns.¹⁸ Yet the control is complex and static, since the surface patterns cannot be provided in dynamic and digital styles. We wish to have a set of available self-organizing components in which the process parameters can be adjusted easily. The instabilities of thin liquid lines have been the subject of increasingly active research aimed at a better understanding of the physics of their

State Key Laboratory of Digital Manufacturing Equipment and Technology, Huazhong University of Science and Technology, Wuhan, 430074, China. E-mail: yahuang@hust.edu.cn; yinzhp@mail.hust.edu.cn

formation and their utility in patterning, organizing, and measuring material properties on the micro and nanoscale.¹⁹ The driving mechanism behind this self-organization is the same gain in surface energy that controls the break-up of liquid lines into droplets that was first explained by Rayleigh.²⁰

A self-organization driven by surface tension and Plateau–Rayleigh instability is presented to directly handle the concentrated functional solution and fabricate large-scale ordered microarrays in a highly-efficient, controllable and digital manner. The finite length effects are utilized to manipulate the self-organizing processes and adjust the self-organization competition between nucleation and free surface instability. Ribbon-lattices are introduced to activate the finite length effects, where the fibres should be deposited with uniform cross-section and arrayed with controlled distances. We present a mechano-electrospinning (MES)-assisted solution-based process to direct-write ribbon-lattices, then transfer the ribbon-lattices to a moisture-rich environment to controllably generate ordered microarrays based on the finite length effects. Traditional electrospinning merely uses an electrical charge to draw micro/nano-scale fibres from a charged liquid, but without being capable of positioning, or being able to control the diameter.^{21–23} MES is different from traditional electrospinning, in that the jetted liquid fibre is pulled by the combination of the stable electrical field force and a tunable mechanical drawing force. This leads to MES being capable of high positioning, direct-writing high-resolution patterns, and controlling the diameter of the jetted fibre/ribbon. The electrical field is utilized to generate the Taylor cone that the jet is pulled from, and also acts as part of the drawing force to pull the jet. The mechanical drawing force is derived from the motion stage and tuned by the velocity of the motion stage, so the diameter of the jet can be controlled by the tunable force. It has high flexibility in manipulating the configuration of fibres directly, such as the diameter and position of fibres, instead of changing the print head. Transferring the ribbon-lattice mask to a solvent-absorbable moisture-rich environment produces modulations to the surface tension, by which the fibres are divided into segments and self-assembled into microarrays or patterns. Surface-tension-driven flows and, in particular, their tendency to decay spontaneously into droplets, have long fascinated naturalists, the earliest systematic experiments dating back to the 19th century.^{20,21} The presented approach combines the advantages of high-controllability of electrohydrodynamic printing and parallel fabrication of self-organization. It is able to fabricate large-scale size/position-controllable microarrays, and is not hampered by the disadvantages encountered with contact approaches and ink-jet printing.

2. Surface-tension driven self-organization

It is essential in self-organization to generate a globally coherent pattern in a way that is parallel and distributed, either from the local direct interactions (*e.g.* by capillary forces²⁴), or indirectly using a template²⁵ or an external field (*e.g.* by kinetic driving,²⁶ electrohydrodynamic instability¹⁹ or laser-interference²⁷). Fig. 1 shows the schematic diagram of surface-tension driven self-organization assisted by mechano-electrospinning. Firstly, MES is presented to direct-write aligned fibres with a diameter of several micrometers/submicrometers on flexible/rigid substrates (Fig. 1(a)). The fibres become ribbons, since the fibres deposited

on the substrate are still liquid when a short nozzle-to-substrate distance is adopted. Then, the samples are exposed to water vapor at a humidity of about 60%, or moist airflow is blown onto the sample (Fig. 1(b)). Water will condense on the substrate surface, which is usually used in “breath figures” to form well-ordered conformal micropatterns.²⁸ The condensed water has an influence on the surface energy, namely reducing the surface energy of Si. Here, the solid ribbon absorbs water-vapor and swells into liquid fibres. Thirdly, the large surface tension resulting from the large specific-surface-area necks the liquid fibres and breaks them into segments (Fig. 1(c)). Surface tension is the force responsible for a variety of physical phenomena involving small volumes of liquid.²⁹ Here, surface tension has demonstrated the capability to cut free-standing liquid micro/nanofibres into a periodic array of fragments, known as Plateau–Rayleigh instability.³⁰ Lastly, the fragments further shrink from the fusiformis-shape into approximately circular droplets in order to minimize their surface area, thus the system generates a great wealth of periodic and hierarchical structures (Fig. 1(d)). The solvent will evaporate and the microarrays will mold at the droplets when the sample is transferred out of the moisture-rich environment. In order to control the self-organization process, the finite length effect is utilized by introducing ribbon-lattices, which act as an induction template and provide high controllability of droplet-size and position.

Closer analysis of our self-organization experiments suggests that two important factors determine the presented self-organization: the moisture-rich environment and the ribbon-lattice. The former factor is adopted to generate surface tension, which can easily be realized using an aging oven. Increasing the water vapor to a humidity of 60% and decreasing the substrate temperature to 5 °C below the dew point form an effective approach to condensing the water onto the wettable hydrophilic regions.³¹ The self-organization begins when enough water is absorbed, and stops when it is transferred out of the moisture-rich environment.

There are two different phenomena responsible for droplet formation: (i) instability of the body of the ribbon itself where the self-organization is carried out freely,²⁷ and (ii) instability induced by the finite length effects, which have been observed and studied in theory and experiment.³² Here, the finite length effects are utilized to control the configuration of droplets, such as their size and position. The challenge is to fabricate large-scale finite length line-arrays at low cost and high throughput. We have presented a solution-based non-contact direct-writing approach named MES to fabricate different kinds of lattices.³³ The lattices contain many square and rectangular cells with specific side lengths, which are anchored by the intersection points at the two ends. The ribbon-lattices are the core of the presented self-organization. The self-organization on the lines will be determined by the length. However, the fabrication of ribbon-lattices is much more difficult than that of ribbons, since the ribbons have to be deposited with uniform width and precise positioning.

3. Ribbon-lattices direct-written by mechano-electrospinning

Here, mechano-electrospinning is presented to form the required ribbon-lattices. Generally, the jetted fibre of traditional

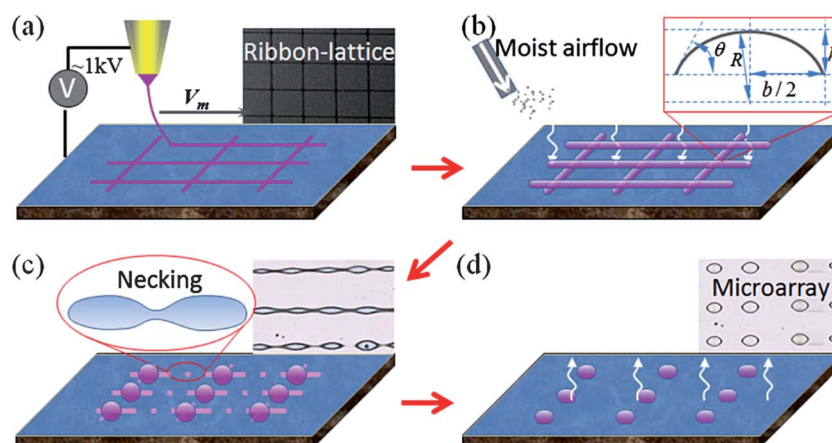


Fig. 1 Schematic diagram of surface-tension driven self-organization assisted by mechano-electrospinning for large-scale microarrays. (a) Fibre-array or ribbon-lattice deposited by MES; (b) the substrate with ribbon-lattice is immersed in moist airflow or blown by moist airflow, and the fibre array swells due to absorbing the water-vapor. The contact width of the liquid line is b , the contact angle is θ , the radius is R , and the thickness of the section line is h . (c) The fibre is necked by surface-tension force. (d) A large-scale ordered microarray is formed.

electrospinning hangs in a similar manner to a rope-ladder swinging from a helicopter, so that it is impossible to control the landing point. To electrodeposit fibre in a controllable manner, the idea is borrowed from the “Chinese kite”, where a person pinches the string and runs quickly. We introduce a high-speed motion stage in the role of the person, to realize controllability of the landing point. Therefore, MES forms fibres based on the uniaxial stretching of a viscoelastic solution, by use of stable electrostatic and tunable mechanical forces. Fig. 2 shows the schematic of the MES process. When a critical electric field is achieved, the electrostatic force will overcome the surface tension of the solution, causing a jet to erupt from the apex of the Taylor cone.³⁴ The formation of the Taylor cone, the jet erupting from the apex, the ink-point deposited on substrate, and the effect of velocity on the orientation of the fibre can be observed.

The substrate is located on an electrode mounted on an x - y motion stage, which can adjust the drawing force acting on the fibre in the flying state, as shown in Fig. 2(c). The motion stage moves rapidly in one direction to generate a mechanical drawing force, and moves in the perpendicular direction in an intermittent manner to adjust the gap. It can be utilized to fabricate ribbon-lattices *in situ*, as the motion stage can move in two perpendicular directions. In order to realize control of the kite, the velocity of the x - y motion stage should be larger than that of the fibre jet. A large velocity leads to a large slope and a large drawing force, which makes the fibres finer, as shown in Fig. 2(d)–(g) captured by a high-speed camera. The liquid jet undergoes extensive stretching as the substrate moves, then attaches onto the substrate in an orderly manner. The mechanical force plays an important role in controlling the diameter and position of the

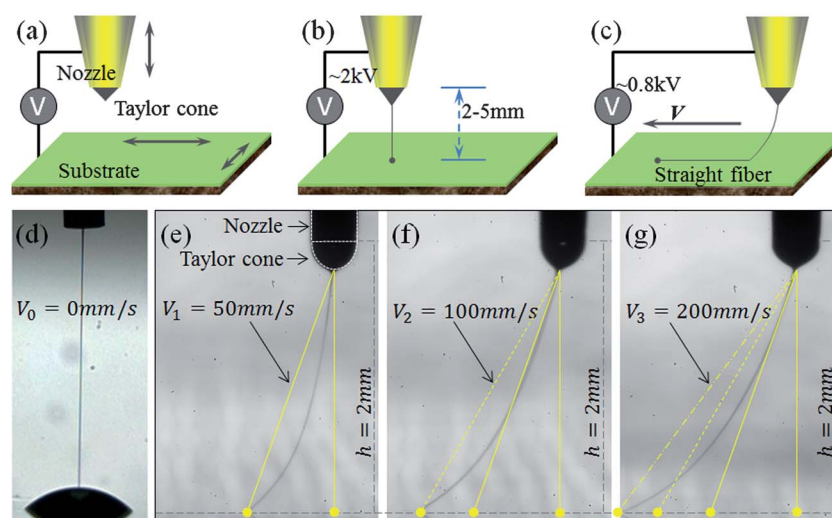


Fig. 2 The processing schematic of MES. The substrate is mounted on an x - y moving stage. The motion stage moves rapidly in one direction to generate the mechanical drawing force, and moves in a perpendicular direction in an intermittent manner to adjust the gap. (a) The nozzle is filled with the solution and a drop forms on the end of the nozzle. (b) The jet emanates from the attached drop and forms the Taylor cone. (c) A fine ‘jet chord’ is formed between the nozzle and the substrate. (d) The fibre is jetted when the motion stage is stationary. (e)–(g) denote the jet when the velocity of the motion stage is 50 mm s^{-1} , 100 mm s^{-1} and 200 mm s^{-1} , respectively. The voltage is 0.8 kV , the distance is 2 mm , and the flow rate is 50 nl min^{-1} .

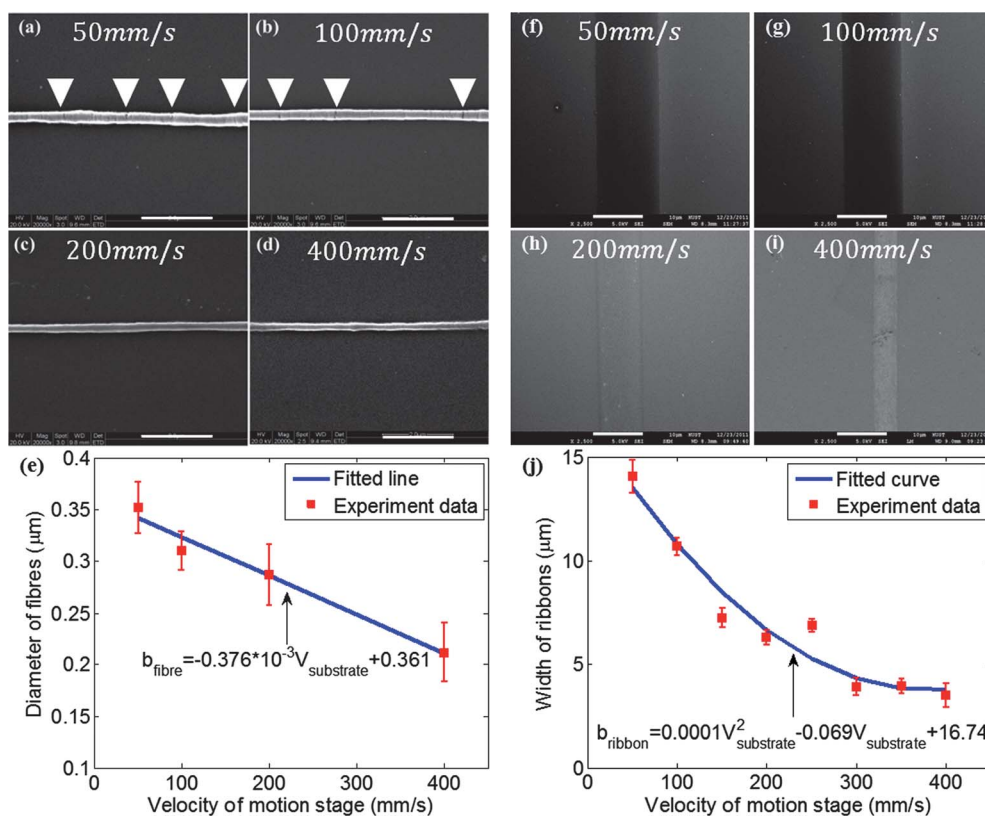


Fig. 3 The fibre-diameter or ribbon-width related to the velocity. (a)–(d) SEM images of the aligned nanofibre with a 5 mm nozzle-to-substrate distance at different velocities of the substrate, including 50 mm s⁻¹, 100 mm s⁻¹, 200 mm s⁻¹ and 400 mm s⁻¹; (e) correlation between the fibre-diameter and the velocity of the motion stage. (f)–(i) SEM images of aligned electrospun nanofibres with a 2 mm nozzle-to-substrate distance at different velocities of the substrate, including 50 mm s⁻¹, 100 mm s⁻¹, 200 mm s⁻¹ and 400 mm s⁻¹; (j) correlation between ribbon-width and velocity of the motion stage. The bars denote 2 μm in (a)–(d) and 10 μm in (f)–(i).

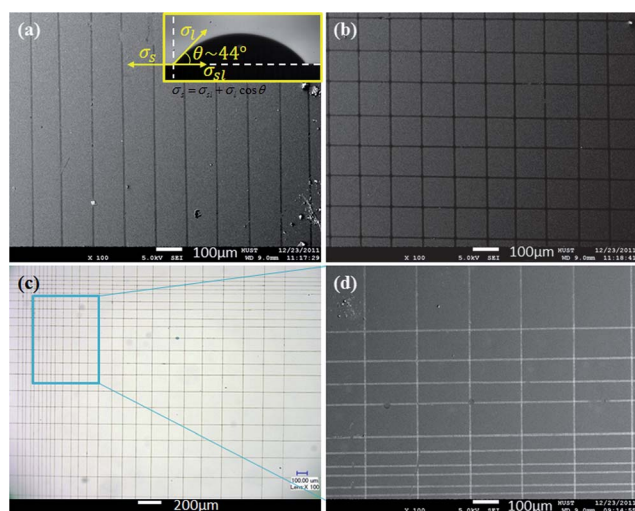


Fig. 4 SEM images and optical microscope image of the ribbon-lattice generated by MES. (a) shows parallel fibres with the same gap, and the top-right box is the image of the contact angle of the solution on the Si substrate; (b) is a ribbon-lattice with the same gap in two directions; (c) and (d) are the optical microscope image and the SEM image of the ribbon-lattice with a gap increasing gradually from 40 μm to 200 μm, respectively.

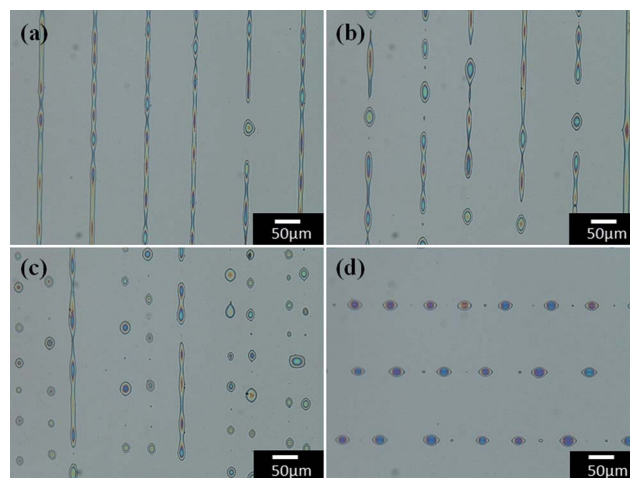


Fig. 5 Optical microscope images of the evolution of self-organization in a moisture-rich environment. (a) The fibres begin necking; (b) the fibres are cut off; (c) the "fusiform-shaped" droplets shrink; (d) the microarray is formed.

electrospun fibres. The nozzle-to-substrate distance ranges from 2–5 mm, far smaller than the 10–30 cm adopted in traditional electrospinning,³⁵ and bigger than the ~0.5 mm adopted in near-field electrospinning.²² The surface properties exert influence on

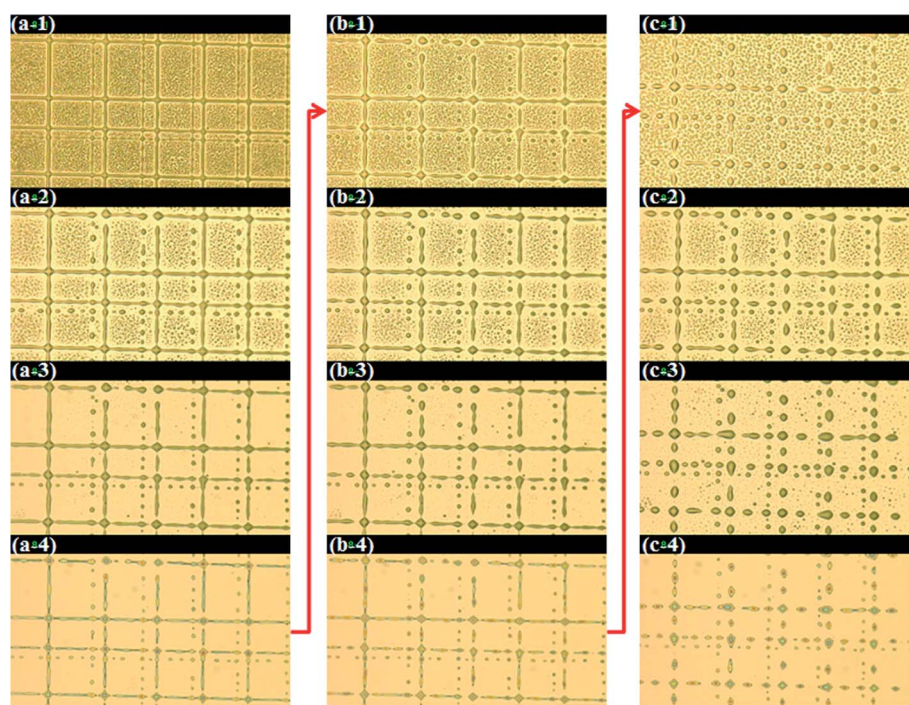


Fig. 6 The effects of the water film on the self-organization. The images are captured from the video by high-speed camera. (a-1)–(a-4) Group (a) shows the first transfer into and out of the moisture-rich environment; (b-1)–(b-4) The sample of Group (b) is the same as that of Group (a). Group (b) is the result of transferring the sample (a-4) into the moisture-rich environment; (c-1)–(c-4) The sample of Group (c) is the same as that of Group (a) and (b). Group (c) is the result of transferring the sample (b-4) into the moisture-rich environment.

the formation of the deposited fibre as well as the morphology of the droplets. However, they have a low influence on the self-organization behavior, which is dominated by surface tension and Plateau–Rayleigh instability.^{36,37} Firstly, the surface energy dominates the interfacial toughness between the substrate and the electrodeposited fibres. In our experiment, we observed that the liquid fibre is deposited on the Si substrate more easily than on a polymeric substrate, such as PI (polyimide) or PDMS (polydimethylsiloxane). Secondly, the surface properties also play an important role in the morphology of the formed droplets, such as the diameter and the height.

Improvements towards control have emerged, including direct-writing nanofibres with controllability of position and fibre-diameter/ribbon-width. It should be emphasized that the positionability and controllability make MES very different from traditional electrospinning, which only collects the fibres in the form of nonwoven fabric. Several features, such as a low applied voltage and a short nozzle-to-substrate distance, and the tunable mechanical drawing of the high-speed motion stage, lead to the ability of MES for positioning and orientation. (1) One of the advantages is to introduce the “near field” into MES. The nozzle-to-substrate distance of 2–5 mm is able to avoid disorderly deposition in traditional electrospinning, and the comparatively low applied voltage also avoids electrical breakdown in near-field electrospinning. The nozzle-to-substrate distance also plays an important role in controlling the phase change of the jetted fibres. If the nozzle-to-substrate distance is greatly shortened from 5 mm to 2 mm, the solvent is unable to evaporate completely, and the jetted fibre will become a thin ribbon when it reaches the substrate, as shown in Fig. 3(e)–(i). The jetted fibres need to be

liquid when contacting the substrate, which generates enough interfacial cohesive force to draw the fine “jet chord”. (2) The high-speed motion stage gives the set-up the capability of direct-writing straight fibres and controlling the diameter of the fibre, and avoiding the direct-writing coil/wave fibres in general near-field electrospinning.^{22,38} (3) A d.c. voltage, 0.5–2 kV from a high-voltage power supply, is applied, which is far smaller than that adopted in electrospinning, electrospinning, and e-jet. Then the applied voltage is gradually decreased to a lower voltage of 0.8 kV, just to keep the Taylor cone stable. The fibre will be jetted through the drawing force resulting from the motion stage, which is helpful in reducing the bending instability of the jet in a high electric field. MES is able to fabricate highly ordered nanofibres with high positional accuracy, and paves the way for fabricating large-scale ordered microarrays by surface-tension driven self-organization.

Fig. 3(a)–(d) and (f)–(i) show SEM micrographs of the morphology of fibres fabricated at the velocities of 50 mm s⁻¹, 100 mm s⁻¹, 200 mm s⁻¹ and 400 mm s⁻¹ respectively. The two groups of images present two kinds of morphology, solid fibres and thin ribbons, which result from different nozzle-to-substrate distances and solution concentrations, 5 mm and 3 wt% for (a)–(d) and 2 mm and 4 wt% for (f)–(i). The jetted fibres will solidify more efficiently when a larger nozzle-to-substrate distance is adopted.³³ It also leads to a significant difference between the diameters of the fibres and the widths of the ribbons deposited on the substrate, as shown in Fig. 3(e) and (j). It can be observed that there exist distinct drawing forces from the statistical laws of fibre diameters *versus* the velocity of the motion stage in Fig. 3(e) and (j).

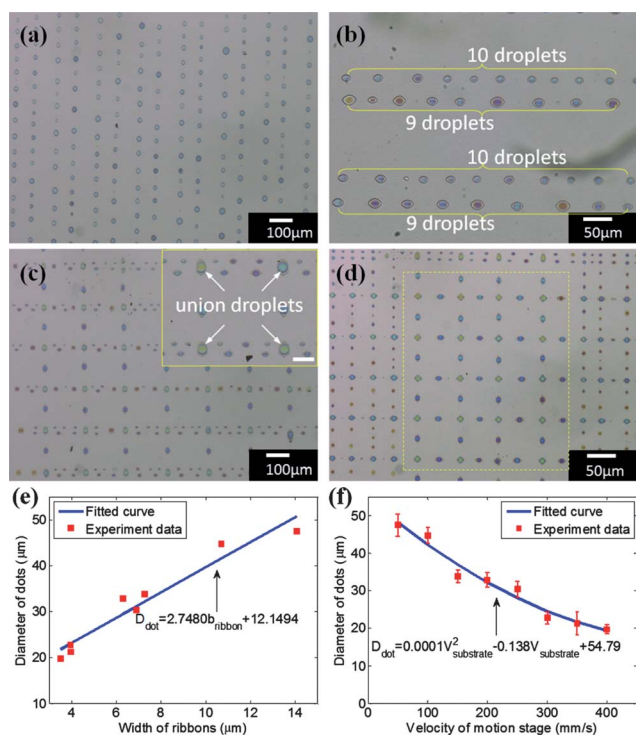


Fig. 7 Optical microscope images to show the effect of ribbon width on the droplet-size. (a) Large scale droplet with uniform width and gap; (b) large scale droplet with uniform width and different gaps; (c) microarray with different widths and gaps, and the bar in the small image denotes 50 μm ; (d) the effects of ribbon width and gap on the density of the droplet; (e) the relationship between diameter of dots and width of ribbons; (f) the relationship between diameter of dots and velocity of the motion stage.

The diameter b_{fibre} or width b_{ribbon} decreases with the regular increase in the velocity $V_{\text{substrate}}$. The linear fitting of the deposited solid fibres is calibrated as $b_{\text{fibre}} = -0.376 \times 10^{-3}V_{\text{substrate}} + 0.361$, and the quadratic fitting of the thin liquid ribbons is calibrated as $b_{\text{ribbon}} = 0.0001V_{\text{substrate}}^2 - 0.0686 \times 10^{-3}V_{\text{substrate}} + 16.739$. Therefore the width of the ribbons (or the diameter of the fibres) can be controlled by adjusting the substrate velocity. It should be stressed that the calibration results vary with the concentration of the solution, the internal diameter of the nozzle, the applied voltage and the nozzle-to-substrate distance. The diameter/width is under control only at specific velocity intervals in which the drawing force successfully stretches the jet. Low velocities, such as those lower than the jetting velocity, are unable to generate a drawing force onto the jetted fibres, yet the jetted fibres will break when the velocity is too high, such as at 800 mm s^{-1} . Cracks are observed on the surface of fibres fabricated at low velocity, highlighted by the white triangles shown in Fig. 3(a) and (b). Conversely, the fibre with a smoother surface can be fabricated by adopting a large velocity. The possible mechanism results from evaporation of the solvent. At low velocity, the fibre with unit length has more solvent, so more solvent will be evaporated from the fibre. It leads to a much more remarkable shrinkage, which is the main reason for the generation of the crack.

One of the advantages of MES over ink-jet printing is that MES can adopt large nozzles to print a fine pattern, and jamming

of the nozzle can be reduced easily. Corresponding to the inner nozzle diameter D_{nozzle} with 160 μm , the *draw-down ratio* R_d is from 465 to 748 for the first group (fibre) and from 11 to 45 for the second group (ribbon), much larger than about 0.3 for ink-jet printing, where $R_d = \frac{D_{\text{nozzle}}}{b_i}$, ($b_i = b_{\text{fibre}}, b_{\text{ribbon}}$). The ink is delivered continuously using a syringe pump at a rate of 50 nL min^{-1} . In addition, the diameters are able to be continuously tuned by the motion stage, this being the specific advantage of MES compared to traditional electrospinning²³ and near-field electrospinning.²²

The configuration of ribbon-lattices plays a dominant role in controlling the droplet-size and droplet-position of the microarray. In order to realize controllability of the microarray with specific position, size and density, ribbon-lattices with different configurations should be designed firstly to meet specific requirements, including the diameter of fibres and the gap between parallel fibres. Fig. 4(a) shows parallel straight fibres with the same gap, which are adopted to show the surface-tension driven self-organization in freedom. One can observe the effect of the ribbon width on the droplet-size and distance between droplets. Fig. 4(b) is the uniform ribbon-lattice, showing the possibility of a large-scale orderly microarray. Fig. 4(c) and (d) are a ribbon-lattice with gradual gap increases from 30 μm to 200 μm , to impose controllability on the formation of the microarray, where Fig. 4(d) is a SEM image showing the partial enlarged detail of an optical microscope image Fig. 4(c). The parallel fibres are used to observe the free self-organization against the diameter of fibres, and the ribbon-lattices are adopted to show the controllability of self-organization. Based on the above patterns, we can fabricate a droplet-array resulting from free self-organization and controllable self-organization, respectively. The ink adopted in experiments is a polyethylene oxide (PEO, $M_w = 300\,000$) solution with weight concentration 4 wt% or 6 wt%. It is dissolved in distilled water, followed by ultrasonic dispersion and magnetic stirring for 10 hours at room temperature. The top-right box of Fig. 4(a) is the contact angle of the PEO solution on the Si substrate. The contact angle is about 44°, which is the average value from dozens of experiments. It is well known to us that $\sigma_s = \sigma_{\text{sl}} + \sigma_l \cos \theta$. The term $(\sigma_s - \sigma_{\text{sl}})$ is called the adhesion tension or wetting tension. It means that the larger the contact angle, the smaller the diameter of the droplets and the greater the height of the droplets.

4. Controllability in self-organization

This section aims at a better understanding of Plateau–Rayleigh instability and the finite length effects and their utility in the controllable formation of microarrays. Fig. 5 shows the dynamic behavior of free self-organization. As the thin ribbons absorb enough water-vapor, they undergo a sudden transition to a morphologically different state. This indicates that surface instabilities are activated. The ribbons are on the micrometer/submicrometer scale, so the solvent evaporates quickly when it is taken away from the moisture-rich environment. The observations suggest that three key elements are required for the self-organization mechanism: (i) the self-organization of free-standing thin ribbons is in an uncontrolled style. The ribbon-lattice is adopted to form a large-scale ordered fibre-array with

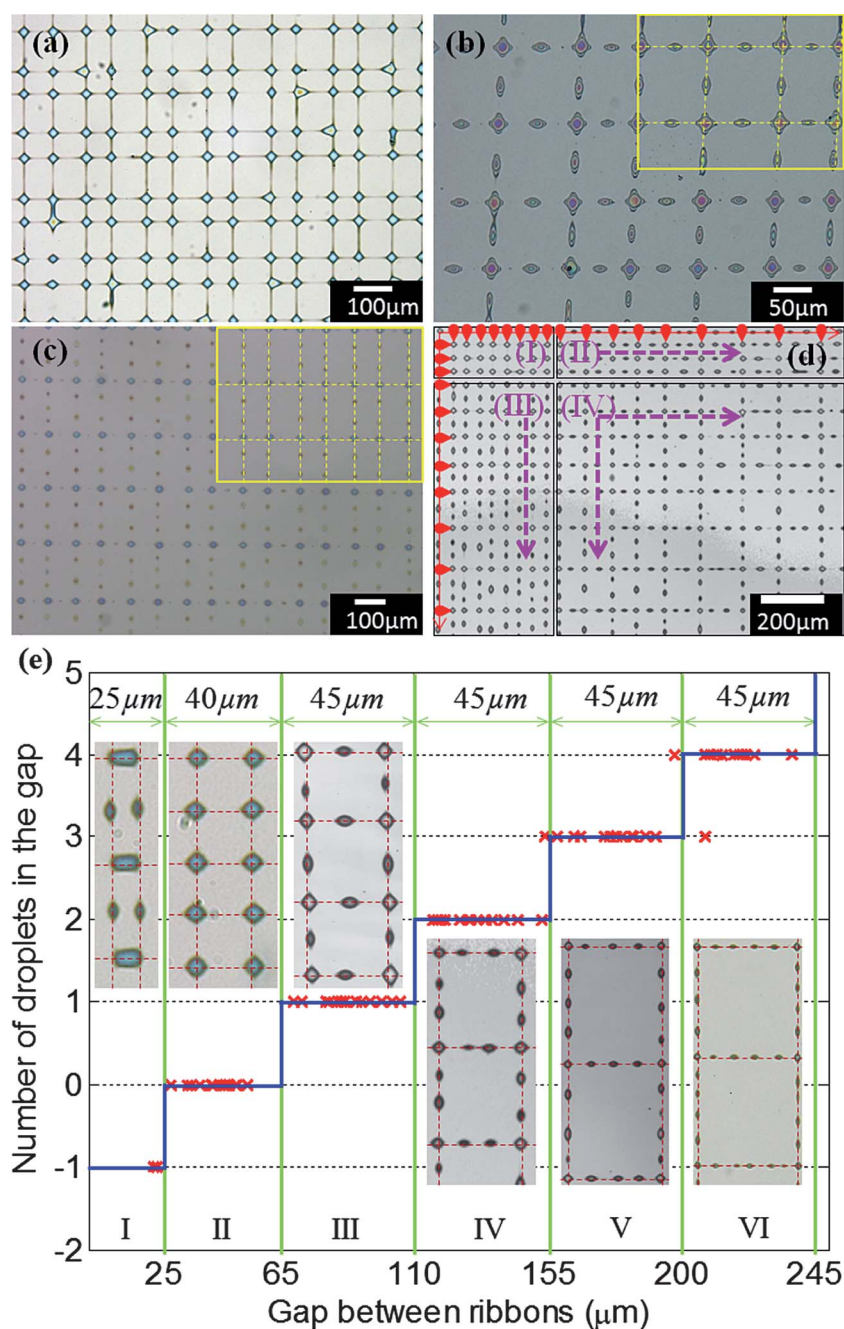


Fig. 8 Optical microscope images to show a highly-uniform droplet-array with different controllable widths. (a) The ribbon-lattice during necking; (b) the ribbon-lattice during shrinking; (c) large-scale uniform microarray with controlled position and volume; (d) image by Laser Scanning Confocal Microscope to show the effect of the gap between ribbons. (e) Relationship between the amount of necking and the gap length between ribbons. The \times denotes experimental data, and the blue solid line is the fitting line. “-1” on the axis of the number of droplets in the gap means that there is no necking and the two intersection points are unified together. The dashed lines in the upper-right rectangular boxes of (b) and (c) and on the images of (e), and the direction of the raindrop arrows in (d) indicate the location of the original ribbons before the break-up process takes place.

high-positionability and high-uniformity; (ii) a suitable-humidity environment is needed for absorbing water-vapor, and a dry environment for quick evaporation; (iii) it needs enough time to finish three obvious sequences of self-organization, including necking, breaking, and contracting. The time is dependent on the width of ribbons and the humidity of the environment. Usually the necking is the most important since it determines the position of breaking, the density of droplets and the droplet size.

Certainly, the humidity of the environment and the temperature of the substrate should collaborate to generate a water film with a suitable thickness. Fig. 6 shows the effects of the water film on the self-organization. When the water is condensed into a thick water film, the ribbon dissolves and diffuses quickly into the water. This leads to a microarray with a large diameter and a small height. In order to improve the controllability, it is better to adopt a thin water film. Fig. 6(a-1)–(a-4) show the sample being

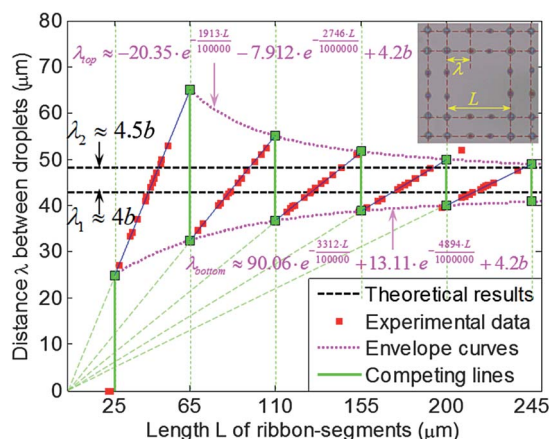


Fig. 9 The distance λ changes with the length L of the ribbon-segments. The controllability of the distance λ is higher when the length L is smaller. The envelope area between the two envelope curves is controllable. $b \approx 10.7 \mu\text{m}$ is the width of the ribbons.

transferred into and out of the moisture-rich environment for the first time. It can be observed that the thin fibres experience necking, cutting off and shrinking, and the entire procedure is finished. However, the thick fibres are not cut off, and are still continuous lines. (a-2) and (a-3) are the intermediate procedures in which the water film is evaporated gradually. In order to finish the self-organization, the sample should be transferred into the moisture-rich environment several times if the water film is too thin. (b-1) is the result of the sample (a-4) transferred into moisture. The degree of self-organization of Group (b) is deeper than that of Group (a). In the same way, (b-4) is transferred into the moisture-rich environment again. And the results of Groups (c) show clearly that the entire procedure of self-organization is finished, even the thick fibres.

Different droplet-sizes are usually required in different applications. However, it is impractical for traditional ink-jet printing/e-jet to deposit various droplet-sizes in a continuously tunable manner by one print head, since it is only able to generate droplets of one size. The MES-assisted self-organization has the capability to generate microarrays with a specific droplet-size and position in a continuously tunable, digital manner. Fig. 7(a)–(d) show the results of the controllability of droplet-size through adjusting the ribbon width. The ribbons are generated by adjusting the velocity of the motion stage according to the calibration relation in Fig. 3(j). Fig. 7(a) and (b) illustrate a large-scale microarray evolved from parallel fibres with uniform diameter and different diameters, respectively. They belong to the self-organization of free-standing ribbons, where the droplet-size is affected by the ribbon width. It can be observed from Fig. 7(b) that the width is in charge of the droplet-size and droplet-distance along the ribbons. The gap between ribbons is another important parameter to control the density of the microarray in the direction perpendicular to the parallel ribbons. This suggests that a dense microarray can be fabricated by reducing the ribbon width and the distance between ribbons.

Fig. 7(c) and (d) show that the droplet-size is adjusted on the basis of a combination of the ribbon-width and the intersection of perpendicular fibres. The ribbon-lattice for Fig. 7(c) is made

up of narrow ribbons in the horizontal direction and wide ribbons in the vertical direction. The biggest droplets are located at the point of intersection. There exist competing morphologies of drops, in particular drop-based “digital” self-organization. When the gap between two ribbons becomes small enough, a complex phenomenon appears, in which the ribbon between the two interaction points is difficult to cut off in the process of necking. The two end points of the ribbon segment will merge together to form “union droplets” due to surface tension, as shown in the enlarged image in Fig. 7(c). Fig. 7(d) shows self-organization of the ribbon-lattices into fine horizontal ribbons in the peripheral region and thick vertical ribbons in the central region. It can generate hierarchical microarrays and give a clear image of the effect of ribbon width and intersection points, as shown in the dashed-line rectangle. Furthermore, whereas the freestanding ribbons will always undergo a Plateau–Rayleigh instability, the droplet turns out to be homogeneous as long as the ribbons are sufficiently uniform. Fig. 7(e) shows that there exists an obvious linear relationship between the droplet diameter at the intersection points and the ribbon width, namely $D_{\text{dot}} = 2.7480b_{\text{ribbon}} + 12.1494$. The relationship of ribbon width, b_{ribbon} , versus velocity of the motion stage, $V_{\text{substrate}}$, was obtained and shown in Fig. 3(j), from which the microarray at a specific droplet-size can be generated directly by MES in a digital manner. It can be observed that the height of the droplet is $\sim 1 \mu\text{m}$, which is not directly dominated by the process parameters, but by the material properties of the solution and substrate. Fig. 7(f) shows the relationship between the diameter of the dot and the velocity of the motion stage, namely $D_{\text{dot}} = 0.0001V_{\text{substrate}}^2 - 0.138V_{\text{substrate}} + 54.79$. The velocity of the motion stage, $V_{\text{substrate}}$, is controlled by numerical computer, so it can be considered as a digital fabrication approach for a large-scale microarray.

Fig. 8 indicates that the droplet position can be controlled precisely at the intersection where self-organized droplets are definitely generated. However, whether there are droplets between fibres depends on the configuration of the ribbon-lattices. The PEO solution with weight concentration 4 wt% is adopted for Fig. 8(a) and (d), and 6 wt% for Fig. 8(b) and (c). There are critical values of gaps for the modes unable to be necked between two interaction points, and those able to be necked once (the condition of no point at the gap), twice (the condition of one point at the gap), and so on. Fig. 8(c) shows the combined influence of the droplet-size and droplet-gap. The small ratio of diameter to gap contributes to generating more droplets, from which the effect of the ratio is able to be validated clearly when two apparently different ratios are compared. If the ribbon-gap is small enough or the ribbon width is big enough, there may be only a big droplet connecting two intersections, and no small droplets located at the gap. This predicts that controlling the interaction between the fibres and the liquid–air interface is the key to the realization of highly ordered droplet-arrays.

In order to observe the finite length effects, one can focus on the microarray in Fig. 8(d), which is self-organized from the ribbon-lattice, with gaps increasing gradually as shown in Fig. 4(c). The image can be divided into 4 parts, named *Areas I, II, III* and *IV*, according to the gap. The microarray in *Area I* has the same sized gap in the horizontal and vertical directions, and there are no tiny droplets in the gap. The self-organized droplets

with the same size are anchored at the intersection points of perpendicular ribbons. *Area II* is different from *Area I* since the vertical gap remains the same while the horizontal gap becomes gradually larger. It is the same with *Area I* in the vertical direction, in that there are no droplets in the gap, however it is different in the horizontal direction, as there are one or more droplets in the gaps. The number of droplets in the gap is determined by the length of the gap, which is considered as the finite length effects adopted to manipulate the self-organization. *Area III* is similar to *Area II* but in the perpendicular direction. In *Area IV* the number of droplets in the gap becomes larger, with the gap increasing in two directions gradually. The evolution of the droplets located at the intersection point is different from in other parts of the fibres. It can be seen in Fig. 5 that the droplet is evolved from an ellipse in free self-organization. However, the droplets located at the intersection points demonstrate four-pointed stars at first, then gradually change into approximately circular droplets. These droplets resulting from two intersectant ribbons are usually bigger than the others in the gap. The intersection points are composed of two segments from two perpendicular ribbons, however the points between gaps are composed of only one segment. Experiments show that the segments for the intersection points are about the same length as the segments for other points in the same sample. It can be concluded from analysis of the experimental data that the volume at the intersection point is about twice as big as in the gap when the two intersectant ribbons have the same cross-section area. It should be emphasized that the droplets, either at or between these intersection points, are formed in high order.

It can be observed from Fig. 8(e) that there exists an obvious relationship between the size of the gap and the number of droplets in the gap. In our experiment there are six areas, from “*Area I*” to “*Area VI*”. In *Area I* there is no necking and the two intersection points are unified together. It means that microarrays are unable to be self-organized when the gap length is smaller than 25 μm in the case of $b_{\text{ribbon}} \approx 10.7 \mu\text{m}$ in our experiments. It is well known that a liquid line on a flat substrate can be unstable, depending on the boundary conditions, and there is a competition between nucleation and surface instability.^{32,39} In *Area II*, there are no droplets in the gap and the self-organized droplets are exactly located at the intersection points. By use of this characteristic, highly ordered and uniform microarrays can be fabricated in a parallel manner; meanwhile the droplet-gap can be continuously tuned from 25 μm to 65 μm . In *Area III*, there is one droplet in each gap, based on which hierarchical microarrays are able to be generated. The droplet-gap can be determined in the interval (65/2 $\mu\text{m} = 32.5 \mu\text{m}$ to 110/2 $\mu\text{m} = 55 \mu\text{m}$). After the gap increases to 110 μm , a new droplet will be added for every 45 μm of the gap. We analyzed the droplets in the gap, which are nearly elliptical in shape, with $24.55 \pm 2.29 \mu\text{m}$ in the long-axis direction and $12.42 \pm 1.42 \mu\text{m}$ in the short-axis direction. We perform a standard linear stability analysis of infinitely long ribbons, and identify the corresponding stable, unstable, and metastable regions. The numerical simulations show that for long and thin ribbons, they generate periodic patterns involving successive formation of droplets or necking. On the other hand, for shorter and thicker ribbons, the evolution ends up by forming a single drop, particularly as shown in *Area I* of Fig. 8(e). The final droplet-pattern shows a competition

between the gathering mechanism caused by nucleation and the necking mechanism by free surface instability.

A ribbon of rectangular cross section with width b_{ribbon} and thickness h_{ribbon} is often the initial state, and the principle is the same area when transforming into a rivulet. The simplified model is shown in Fig. 1(b), where the thin ribbons absorb water-vapor and become static rivulets with circular parts cross-sectioned on a horizontal plate. The contact width b approximates the width b_{ribbon} , contact angle is θ , radius is R , and the thickness of the section line h is much larger than h_{ribbon} . For micro beads, gravity is neglected as the bond number is small. For the final droplet array, Brochard-Wyart and Redon³⁶ studied the varicose modes of a liquid rim deposited on a flat solid surface, giving the simple result that the wavelength λ is directly proportional to the width, $\lambda \approx 4b$. Kondic *et al.*³⁷ give the result that $\lambda \approx 4.5b$, where the result is based on the Ni line on the Si substrate, and the contact angle is approximately $\pi/2$.

The finite length effects are able to make the droplet-gap deviate from self-organization in the free state. It can be observed from Fig. 9 that there are obvious finite length effects when the distance L is small. We utilized the finite length effect to manipulate the self-organization behavior, and the region between the two envelope curves is controllable. The distance λ between droplets continually approaches the theoretical prediction, which does not consider the finite length effects. With the distance L increasing gradually, the finite length effects become inconspicuous. Meanwhile, the controllability of the self-organization is weakened gradually. There is a competing patterning denoted by the green competing lines. There exists a competition behavior at the critical length L . When the length L passes through the green competing lines, the distance λ suddenly reduces and the number of droplets jumps immediately. In our experiments $b \approx b_{\text{ribbon}} \approx 10.7 \mu\text{m}$, so we can get $\lambda_1 = 42.8 \mu\text{m}$ or $\lambda_2 = 48.2 \mu\text{m}$ according to the studies of Brochard-Wyart *et al.*³⁶ and Kondic *et al.*,³⁷ respectively. The periodic jump appears every 45 μm in our experiment, located in an interval between λ_1 and λ_2 . Based on the experimental data, we can get the upper limit of the droplet-gap $\lambda_{\text{bottom}} \approx 90.06e^{-\frac{3312L}{100000}} + 13.11e^{-\frac{4894L}{1000000}} + 4.2b$, and the lower limit $\lambda_{\text{top}} \approx -20.35e^{-\frac{1913L}{100000}} - 7.912e^{-\frac{2746L}{1000000}} + 4.2b$, by virtue of the curve-fitting technique. It can be analyzed that the distance λ can be tuned by the length L and the width b . With the infinite increase of the length L , it can be calculated in the limit that λ tends to $4.2b$ ($\lambda/b = 45/10.7 \mu\text{m} \approx 4.2 \mu\text{m}$), between $4b$ ³⁶ and $4.5b$.³⁷ The experimental data coincide with the theoretical results perfectly. When the length L becomes large, the finite length effects will disappear gradually, and the distance λ converges to the theoretical results, namely the controllability deteriorates.

5. Conclusions

We have shown an alternative method to digitally fabricate large-scale microarrays through mechano-electrospinning-assisted surface-tension driven self-organization. Plateau-Rayleigh instability and the finite length effects are utilized to manipulate the self-organization processes and adjust the competition between nucleation and free surface instability. The findings of the present study open up the possibility of being able to deposit large-scale, controllable, highly ordered microarrays for a range

of engineering applications. Unlike the situation with ink-jet printing, mechano-electrospinning has the capability of continuously adjusting the minimum droplet size in a digital manner. This nonlithographic approach is especially appealing because of the potential for low cost in large-scale production. The surface-selective deposition enabled all-solution-processed fabrication of large-scale droplet arrays, making them an advantageous candidate for the fabrication of sensors, optical devices and magnetic storage media.

Acknowledgements

The authors acknowledge the Natural Science Foundation of China (51175209, 51035002) and the Fundamental Research Funds for the Central Universities (2011TS024).

References

- 1 T. W. Kelley, P. F. Baude, C. Gerlach, D. E. Ender, D. Muires, M. A. Haase, D. E. Vogel and S. D. Theiss, Recent progress in organic electronics: materials, devices, and processes, *Chem. Mater.*, 2004, **16**, 4413–4422.
- 2 C. T. Black, R. Ruiz, G. Breyta, J. Y. Cheng, M. E. Colburn, K. W. Guarini, H. C. Kim and Y. Zhang, Polymer self assembly in semiconductor microelectronics, *IBM J. Res. Dev.*, 2007, **55**, 605–633.
- 3 T. Minari, C. Liu, M. Kano and K. Tsukagoshi, Controlled self-assembly of organic semiconductors for solution-based fabrication of organic field-effect transistors, *Adv. Mater.*, 2012, **24**, 299–306.
- 4 B. Y. Chow, C. J. Emig and J. M. Jacobson, Photoelectrochemical synthesis of DNA microarrays, *Proc. Natl. Acad. Sci. U. S. A.*, 2009, **106**, 15219–15224.
- 5 J. Viventi, D. H. Kim, L. Vigeland, E. S. Frechette, J. A. Blanco, Y. S. Kim, A. E. Avrin, V. R. Tiruvadi, S. W. Hwang, A. C. Vanleer, D. F. Wulsin, K. Davis, C. E. Gelber, L. Palmer, J. Van der Spiegel, J. Wu, J. L. Xiao, Y. G. Huang, D. Contreras, J. A. Rogers and B. Litt, Flexible, foldable, actively multiplexed, high-density electrode array for mapping brain activity *in vivo*, *Nat. Neurosci.*, 2011, **14**, 1599–1605.
- 6 N. Berthet, I. Leclercq, A. Dublineau, S. Shigematsu, A. M. Burguiere, C. Filippone, A. Gessain and J. C. Manuguerra, High-density resequencing DNA microarrays in public health emergencies, *Nat. Biotechnol.*, 2010, **28**, 25–27.
- 7 X. Fan, E. K. Lobenhofer, M. Chen, W. Shi, J. Huang, J. Luo, J. Zhang, S. J. Walker, T.-M. Chu, L. Li, R. Wolfinger, W. Bao, R. S. Paules, P. R. Bushel, J. Li, T. Shi, T. Nikolskaya, Y. Nikolsky, H. Hong, Y. Deng, Y. Cheng, H. Fang, L. Shi and W. Tong, Consistency of predictive signature genes and classifiers generated using different microarray platforms, *Pharmacogenomics J.*, 2010, **10**, 247–257.
- 8 H. J. Fan, P. Werner and M. Zacharias, Semiconductor nanowires: from self-organization to patterned growth, *Small*, 2006, **2**, 700–717.
- 9 W. K. Huang, C. J. Ko and F. C. Chen, Organic selective-area patterning method for microlens array fabrication, *Microelectron. Eng.*, 2006, **83**, 1333–1335.
- 10 R. D. Piner, J. Zhu, F. Xu, S. Hong and C. A. Mirkin, “Dip-pen” nanolithography, *Science*, 1999, **283**, 661–663.
- 11 Y. N. Xia and G. M. Whitesides, Soft lithography, *Angew. Chem., Int. Ed.*, 1998, **37**, 551–575.
- 12 H. Sirringhaus, T. Kawase, R. H. Friend, T. Shimoda, M. Inbasekaran, W. Wu and E. P. Woo, High-resolution ink-jet printing of all-polymer transistor circuits, *Science*, 2000, **290**, 2123–2126.
- 13 Z. P. Yin, Y. A. Huang, N. B. Bu, X. M. Wang and Y. L. Xiong, Ink-jet printing for flexible electronics: materials, processes and equipments, *Chin. Sci. Bull.*, 2010, **55**, 3383–3407.
- 14 B. J. de Gans, P. C. Duineveld and U. S. Schubert, Ink-jet printing of polymers: state of the art and future developments, *Adv. Mater.*, 2004, **16**, 203–213.
- 15 J. U. Park, M. Hardy, S. J. Kang, K. Barton, K. Adair, D. K. Mukhopadhyay, C. Y. Lee, M. S. Strano, A. G. Alleyne, J. G. Georgiadis, P. M. Ferreira and J. A. Rogers, High-resolution electrohydrodynamic jet printing, *Nat. Mater.*, 2007, **6**, 782–789.
- 16 R. Bitar, G. Agez and M. Mitov, Cholesteric liquid crystal self-organization of gold nanoparticles, *Soft Matter*, 2011, **7**, 8198–8206.
- 17 G. M. Whitesides and B. Grzybowski, Self-assembly at all scales, *Science*, 2002, **295**, 2418–2421.
- 18 P. Lenz and R. Lipowsky, Morphological transitions of wetting layers on structured surfaces, *Phys. Rev. Lett.*, 1998, **80**, 1920–1923.
- 19 X. Xi, D. Zhao, F. Tong and T. Cao, The self-assembly and patterning of thin polymer films on pyroelectric substrates driven by electrohydrodynamic instability, *Soft Matter*, 2012, **8**, 298–302.
- 20 L. Rayleigh, On the capillary phenomena of jets, *Proc. R. Soc. London*, 1879, **29**, 71–97.
- 21 D. H. Reneker and A. L. Yarin, Electrospinning jets and polymer nanofibers, *Polymer*, 2008, **49**, 2387–2425.
- 22 D. Sun, C. Chang, S. Li and L. Lin, Near-field electrospinning, *Nano Lett.*, 2006, **6**, 839–842.
- 23 W. E. Teo and S. Ramakrishna, A review on electrospinning design and nanofibre assemblies, *Nanotechnology*, 2006, **17**, R89–R106.
- 24 K. Y. Suh and H. H. Lee, Capillary force lithography: large-area patterning, self-organization, and anisotropic dewetting, *Adv. Funct. Mater.*, 2002, **12**, 405–413.
- 25 M. Rycenga, P. H. C. Camargo and Y. N. Xia, Template-assisted self-assembly: a versatile approach to complex micro- and nanostructures, *Soft Matter*, 2009, **5**, 1129–1136.
- 26 T. P. Bigioni, X. M. Lin, T. T. Nguyen, E. I. Corwin, T. A. Witten and H. M. Jaeger, Kinetically driven self assembly of highly ordered nanoparticle monolayers, *Nat. Mater.*, 2006, **5**, 265–270.
- 27 C. Favazza, J. Trice, R. Kalyanaraman and R. Sureshkumar, Self-organized metal nanostructures through laser-interference driven thermocapillary convection, *Appl. Phys. Lett.*, 2007, **91**, 0431051.
- 28 L. Li, Y. W. Zhong, J. L. Gong, J. A. Li, C. K. Chen, B. R. Zeng and Z. Ma, Constructing robust 3-dimensionally conformal micropatterns: vulcanization of honeycomb structured polymeric films, *Soft Matter*, 2011, **7**, 546–552.
- 29 R. R. A. Syms, E. M. Yeatman, V. M. Bright and G. M. Whitesides, Surface tension-powered self-assembly of microstructures: the state-of-the-art, *J. Microelectromech. Syst.*, 2003, **12**, 387–417.
- 30 J. Eggers, Nonlinear dynamics and breakup of free-surface flows, *Rev. Mod. Phys.*, 1997, **69**, 865–929.
- 31 H. Gau, S. Herminghaus, P. Lenz and R. Lipowsky, Liquid morphologies on structured surfaces: from microchannels to microchips, *Science*, 1999, **283**, 46–49.
- 32 J. A. Diez and L. Kondic, On the breakup of fluid films of finite and infinite extent, *Phys. Fluids*, 2007, **19**, 0721071.
- 33 N. B. Bu, Y. A. Huang, X. M. Wang and Z. P. Yin, Continuously tunable and oriented nanofiber direct-written by mechano-electrospinning, *Mater. Manuf. Processes*, 2012, DOI: 10.1080/10426914.2012.700145.
- 34 H. K. Choi, J. U. Park, O. O. Park, P. M. Ferreira, J. G. Georgiadis and J. A. Rogers, Scaling laws for jet pulsations associated with high-resolution electrohydrodynamic printing, *Appl. Phys. Lett.*, 2008, **92**, 1231091–1231093.
- 35 Z. M. Huang, Y. Z. Zhang, M. Kotaki and S. Ramakrishna, A review on polymer nanofibers by electrospinning and their applications in nanocomposites, *Compos. Sci. Technol.*, 2003, **63**, 2223–2253.
- 36 F. Brochard-Wyart and C. Redon, Dynamics of liquid rim instabilities, *Langmuir*, 1992, **8**, 2324–2329.
- 37 L. Kondic, J. A. Diez, P. D. Rack, Y. F. Guan and J. D. Fowlkes, Nanoparticle assembly *via* the dewetting of patterned thin metal lines: understanding the instability mechanisms, *Phys. Rev. E: Stat., Nonlinear, Soft Matter Phys.*, 2009, **79**, 026302.
- 38 C. Hellmann, J. Belardi, R. Dersch, A. Greiner, J. H. Wendorff and S. Bahnmüller, High Precision deposition electrospinning of nanofibers and nanofiber nonwovens, *Polymer*, 2009, **50**, 1197–1205.
- 39 P. C. Duineveld, The stability of ink-jet printed lines of liquid with zero receding contact angle on a homogeneous substrate, *J. Fluid Mech.*, 2003, **477**, 175–200.